



PERGAMON

Available online at www.sciencedirect.com

SCIENCE @ DIRECT®

Acta Astronautica 56 (2005) 652–669

ACTA
ASTRONAUTICA

www.elsevier.com/locate/actaastro

Trajectory correction manoeuvres in the transfer to libration point orbits

Gerard Gómez^{a,*}, Manuel Marcote^a, Josep J. Masdemont^b

^aIEEC & Departament de Matemàtica Aplicada i Anàlisi, Universitat de Barcelona, Gran Via 545, 08007 Barcelona, Spain

^bIEEC & Departament de Matemàtica Aplicada I, Universitat Politècnica de Catalunya, Diagonal 647, 08028 Barcelona, Spain

Received 20 June 2003; received in revised form 28 September 2004; accepted 22 November 2004

Abstract

In this paper we study the manoeuvres to be done by a spacecraft in order to correct the error in the execution of the injection manoeuvre in the transfer trajectory. We will consider the case where the nominal trajectory is a halo orbit around the collinear equilibrium point L_1 . The results can be easily extended to the L_2 point and to other kinds of libration point orbits, such as Lissajous and quasi-halo orbits. For our study we use simple dynamical systems concepts related with the invariant manifolds of the target orbit, and we compare our results with those obtained by Serban et al. (Automatica, 38(2002) 571) using optimal control.

© 2005 Elsevier Ltd. All rights reserved.

1. Introduction

This paper is devoted to the study of the so called trajectory correction manoeuvres (TCM) problem, that deals with the manoeuvres to be done by a spacecraft in the transfer segment between the parking orbit and the target nominal one. The main purpose of the TCMs is to correct the error introduced by the injection manoeuvre in the transfer trajectory due to the inaccuracies of the launch vehicle.

In connection with the Genesis mission (see [10]), the TCM problem has been studied in [8,13]. For this mission, a halo type orbit around the L_1 point of the Earth–Sun system is used as nominal orbit. Since this orbit has a strong hyperbolic character, following the ideas introduced in [4,6], it is possible to use its stable manifold for the transfer, avoiding the insertion manoeuvre into the halo orbit. This is what is known in the literature as the *dynamical systems approach to the transfer problem*. Other approaches use straight-forward propagation from Earth launch conditions to find orbits between the Earth and the halo orbits, keeping some boundary conditions and constraints, at the same time that minimise the total fuel consumption during the transfer (see [3,7,9,11]). In any case, the

* Corresponding author. Tel.: +34 934021651.

E-mail addresses: gerard@maia.ub.es (G. Gómez), marcote@maia.ub.es (M. Marcote), josep@barquins.upc.edu (J.J. Masdemont).

insertion manoeuvre from a parking orbit around the Earth to the transfer trajectory, is a rather large one, with a Δv of the order of 3000 m/s. For the Genesis mission, the error in its execution was expected to be about a 0.2% of Δv (1 sigma value) and a key point to be studied is how large is the cost of the correction of this error when the execution of the first correction manoeuvre is delayed.

For the purpose of comparison, in the present study we will use for the main parameters the same values used by Serban et al. in [13]. More concretely, we will take as reference model for the simulations the restricted three body problem (RTBP) with the value of the mass ratio $\mu = 0.3035910 \times 10^{-5}$ consequently, the gravitational effect of the Moon on the transfer trajectory will not be considered (see [4]). We will also use the same launch conditions near the Earth, which are given in Table 1.

Since the target halo orbit is not explicitly given in [13], we have used one with approximately the same size as the one displayed in the figures of that paper, this is a halo periodic orbit with normalised z -amplitude (see [12] for the definition) $\beta = 0.28$ (approximately 367 000 km) and with initial conditions: $x(0) = -0.9922709412937017$, $y(0) = 0$, $z(0) = -0.002456251256325228$, $\dot{x}(0) = 0$, $\dot{y}(0) = 0.01191138815471799$, $\dot{z}(0) = 0$. It must be noted that the value of the Jacobi constant of the halo orbit, $C = 3.000771793017166$, and the one of the above initial conditions for the transfer, $C = 3.000782265790755$, do not agree. This means, in particular, that the reference transfer trajectory with the initial conditions given in Table 1, is not an orbit of the stable manifold of the halo periodic orbit. Nevertheless, approximately 110 days after launch, the transfer orbit is very close to the halo one and, at that point, a manoeuvre of about 13.5 m/s inserts the spacecraft into the halo. Of course, this insertion manoeuvre could be skipped if the reference initial conditions would belong to the stable manifold but, unfortunately, the departure point rarely meets the constraints associated with actual launch conditions.

In Fig. 1 we have displayed the solution with the initial conditions given in Table 1 as well as the nominal halo orbit. In Fig. 2 we show the different coordinate projections of both the reference transfer trajec-

tory and some “nearby” orbits of the stable manifold of the nominal halo orbit.

In the paper by Serban et al. [13], two different strategies are considered to solve the TCM problem: the *halo orbit insertion* (HOI) technique and the *manifold orbit insertion* (MOI) technique. For the HOI technique, an insertion point in the halo orbit is fixed, in this way at least two manoeuvres must be done: the first one (TCM1) a few days after the departure and the last one at the HOI point. It is numerically shown that, in practice, the optimal solution can be obtained with just two TCMs, so the TCM2 is performed at the HOI point. The time of flight is not fixed in the simulations and, for the optimal costs obtained, it is found that the cost behaves almost linearly with respect to both TCM1 epoch and launch velocity error. The halo orbit insertion time is relatively close (with variations of the order of 20%) to that of the *reference transfer trajectory* (defined as the transfer trajectory with no insertion error). For the MOI approach, the last manoeuvre is an insertion on the stable manifold of the nominal halo orbit, so there is no manoeuvre of insertion onto the halo orbit. The numerical results obtained with this approach are very close to the ones corresponding to the HOI technique. The main technical tool used through the paper is, as in the classical approach to the transfer problem, an optimisation procedure: the software package COOPT, developed at the University of Santa Barbara [14]. This software is used in order to perform an optimisation of the cost function (total Δv) subject to the constraints imposed by the equations of motion. In the same reference, a parametric study of the cost of the TCM is done changing and delaying the execution of the first impulse.

In the present paper we have done the same kind of parametric study as in [13] but without using any optimal control procedure. The quantitative results, concerning the optimal cost of the transfer and its behaviour as a function of the different free parameters, turn out to be the same. Additionally, we provide information on the cost of the transfer when the correction manoeuvres cannot be done at the optimal epochs. These results are qualitatively very close to those obtained in [16] for the cost of the transfer to a Lissajous orbit around L_2 , when the time of flight between departure and the injection in the stable manifold is fixed, but the target state (position and velocity) on the

Table 1

Adimensional initial conditions for the reference transfer trajectory (from [13])

$x_0^{\text{nom}} = -1.000035565608365E + 0$	$\dot{x}_0^{\text{nom}} = 1.547585875645079E - 1$
$y_0^{\text{nom}} = -1.298950527135473E - 5$	$\dot{y}_0^{\text{nom}} = -3.157800035860918E - 1$
$z_0^{\text{nom}} = -1.657172577465346E - 5$	$\dot{z}_0^{\text{nom}} = -1.167438053370118E - 1$

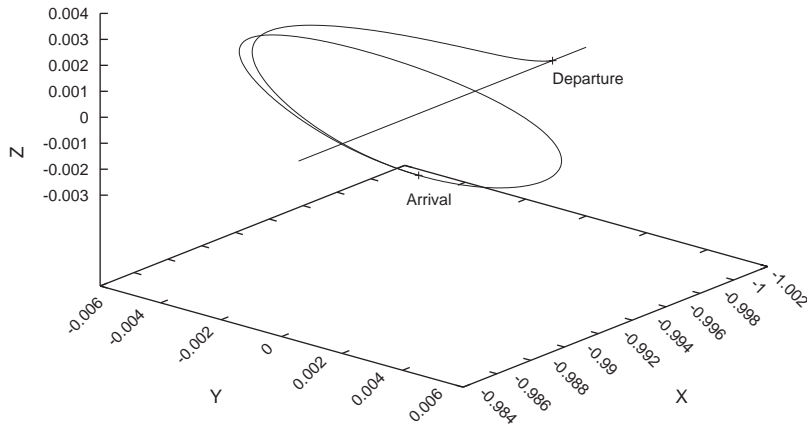


Fig. 1. Reference transfer trajectory and nominal halo orbit, as given in [13], for the study of the TCM problem (adimensional units). The departure and arrival points are separated, approximately 110 days of time of flight.

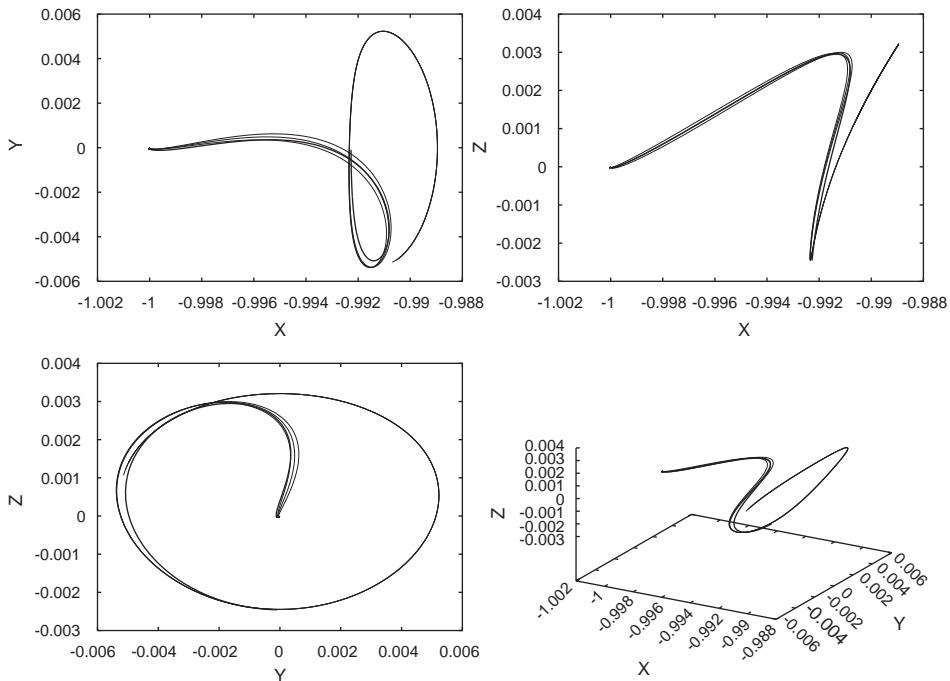


Fig. 2. Projections and three-dimensional (3D) representation of the transfer trajectory used in [13] and “nearby” orbits on the stable manifold of the nominal halo orbit (RTBP units).

manifold is varied. For this problem it is found that the cost of the transfer can rise dramatically, as will be shown. Finally, in Section 4, we will summarise the results of the Monte-Carlo simulations when we allow variations not only in the modulus of the injection velocity but also in its direction.

2. Description of the method

Through all the paper, the initial conditions given in Table 1 have been used as the reference departure state, so the motion will always start from the initial position (close to the Earth) given by this reference point. For the injection error, we have done two kinds of simulations: in the first one, following [13] we only modify the modulus of the velocity at the departure according to

$$\vec{v}(0) = \vec{v}_0^{\text{ref}} \left(1 + \frac{\varepsilon}{\|\vec{v}_0^{\text{ref}}\|} \right). \quad (1)$$

where ε is a parameter that it is allowed to vary between -6 m/s and $+6\text{ m/s}$, and $\vec{v}_0^{\text{ref}} = (-4.612683390613825, 9.412034579485869, -3.479627336419212)^T \text{ km/s}$, which, in adimensional units, correspond to the values given in Table 1. For the simulations of Section 4, we have modified the velocity of the initial condition using

$$\vec{v}(0) = \vec{v}_0^{\text{ref}} + \Delta\vec{v}_0,$$

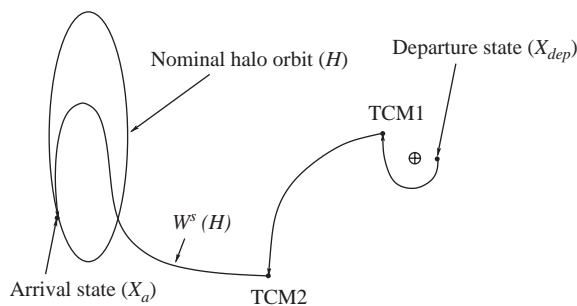


Fig. 3. The three legs used for the computation of the transfer solutions.

where $\Delta\vec{v}_0$ is a point in an ellipsoid with semi-axes $a = \alpha\sigma$, $b = \beta k\sigma$,

being α and β random numbers with $N(0, 1)$ distribution and σ, k two parameters. With this second procedure, we have performed Monte-Carlo simulations with different points of $\Delta\vec{v}_0$ on the ellipsoid.

As it has already been mentioned, in any case, the departure point (X_{dep}) is not on the stable manifold of the nominal halo orbit selected, but rather close to it.

The transfer path has three different legs, qualitatively represented in Fig. 3:

- The first leg goes from the fixed departure point to the point where the TCM1 is performed. Usually, this correction manoeuvre takes place few days after the departure.
- The second leg, between the two trajectory correction manoeuvres TCM1 and TCM2, is used to perform the injection in the stable manifold of the nominal orbit $W^s(H)$.
- The last path corresponds to a piece of trajectory on the stable manifold. Since both TCM1 and TCM2 are assumed to be done without errors, the spacecraft will reach the nominal halo orbit, H , without any additional impulse.

Due to the autonomous character of the RTBP, the origin of time can be arbitrarily chosen. We assume that at departure $t = 0$. As it is explained later, we will select an “arrival point” to the halo. In this way, the TCM1, TCM2 and arrival epochs, will be denoted by t_1, t_2 and t_3 , respectively. The values of the correction manoeuvres at t_1 and t_2 will be denoted by Δv_1 and Δv_2 , respectively.

When we say that we reach the nominal halo orbit, we mean that we are within a certain distance of a point of it, in the direction of the stable manifold. More precisely, this means that if we select a certain (short) distance, d , and an arrival point on the halo, X_a^h , the point that in fact we reach is $X_a = X_a^h + dV^s(X_a^h)$, where $V^s(X_a^h)$ is the linear approximation of the stable direction at the point X_a^h . A value of $d = 200 \text{ km}$ gives good results as is shown in [4]. We remark that the stable manifold is a two-dimensional manifold (a surface in the six-dimensional space of positions and velocities) which can be parametrised in the following way: once a displacement d has been selected,

given a point X^h on the halo orbit we can get an initial condition on the stable manifold $X^h + dV^s(X^h)$. Following the flow backwards we get all the points in the manifold associated with X^h . In this way X^h can be thought as one of the parameters which generate the manifold. In what follows, we will call it the *parameter along the orbit*. The other one is the elapsed time, following the flow, from the initial condition $X_a = X_a^h + dV^s(X_a^h)$ to a certain point. We will refer to this time interval as the *parameter along the flow*. We remark that this parametrisation depends on the choice of d , a small change in d produces an effect equivalent to a small change in the parameter along the orbit. This is: with a small change in d we can get the same orbits of the manifold as with a small change of X^h and only a small shift in the parameter along the orbit will be observed. This is because the stable direction is transversal to the flow.

We denote by $\phi(X, t)$ the image of the point X under the flow of the RTBP after t time units. Given the departure state, X_{dep} , and the time t_1 , we define $X_1 = \phi(X_{\text{dep}}, t_1)$. Then, the transfer condition is stated as

$$\phi(X_1 + \Delta v_1, t_2 - t_1) + \Delta v_2 = \phi(X_a, t_2 - t_3), \quad (2)$$

where, in this relation, a term like $X_1 + \Delta v_1$ has to be understood as: to the state X_1 (position and velocity) we add Δv_1 to the velocity. Note that for a given insertion error (which determines X_{dep}) we have six equality constraints, corresponding to the position and velocity Eq. (2), and 10 parameters: $t_1, t_2, t_3, \Delta v_1, \Delta v_2$ and X_a (given by the parameter along the orbit) which should be chosen in an optimal way within mission constraints.

The sketch of the exploration procedure is the following. To start with, we consider the error ε (or $\Delta \vec{v}^0$) and t_1 fixed. Two types of explorations appear in a natural way: the fixed time of flight transfers, for which t_3 is fixed, and the free time of flight transfers, where t_3 is allowed to vary. In both cases, we start the exploration fixing an initial value for the parameter along the orbit, X_a . In the case of fixed time of flight, the problem then reduces to seven parameters ($t_2, \Delta v_1, \Delta v_2$) and the six constraints (2). Using Δv_1 and Δv_2 to match the constraints (2), the cost of the transfer, $\|\Delta v\| = \|\Delta v_1\| + \|\Delta v_2\|$, is seen as a function of t_2 . In the case of free time of flight, $\|\Delta v\|$ is seen as a

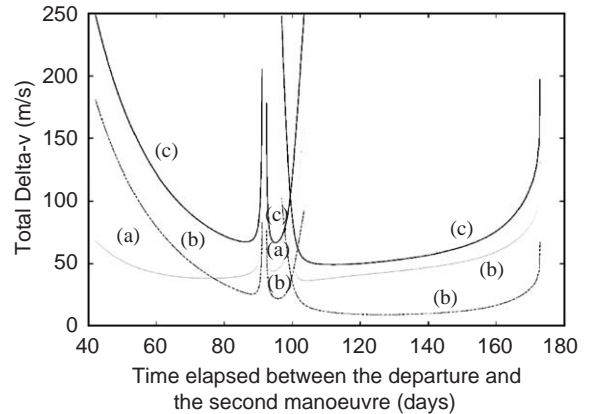


Fig. 4. Cost of the trajectory correction manoeuvres when TCM1 is delayed 4 days after departure and the total time of flight is fixed to 173.25 days. The arrival point on the nominal halo orbit is given in Table 2. The curves labelled with (a) correspond to $\|\Delta v_1\|$, those with (b) to $\|\Delta v_2\|$ and those with (c) to the total cost: $\|\Delta v_1\| + \|\Delta v_2\|$.

function of t_2 and t_3 , or equivalently, as a function of t_2 and the parameter along the flow, $t_{\text{ws}} = t_3 - t_2$.

Once we have explored the dependence of the transfer cost with respect to t_2 and t_3 , we study the behaviour moving the parameter along the orbit, X_a , and finally, the dependence with respect to the error (which is determined by the launch vehicle) and t_1 (which, due to mission constraints, is enough to vary in a narrow and coarse range). We will see that we have some simple linear relations between them.

In order to solve Eq. (2) using a differential correction procedure, we need an initial guess. This is taken from the solution obtained when $\varepsilon = 0$ or $\Delta \vec{v}^0 = 0$. For most of the simulations, as well as for the parametric study, we use a continuation procedure to get the initial approximation of the solution. It must also be noted, that due to the strong hyperbolic behaviour of the orbits under consideration, it can be necessary to solve Eq. (2) using some multiple shooting method (see [15]). We could use a slight variation of the multiple shooting procedure to recover the MOI technique with more than two TCM used in [13], although this possibility has not been implemented.

As a first example, Fig. 4 shows the results obtained when: $\varepsilon = -3$ m/s, the first manoeuvre is delayed 4 days after the departure ($t_1 = 4$), the total time of flight, t_3 , is taken equal to 173.25 days and the arrival point

Table 2

Approximation used for the adimensional coordinates of the arrival point, X_a , of the optimal solution

$x_a = -9.8985625832629109E - 1$	$\dot{x}_a = 3.3913736319571984E - 3$
$y_a = 4.1836615583455538E - 3$	$\dot{y}_a = -6.2057458211230666E - 3$
$z_a = 2.1771475345925264E - 3$	$\dot{z}_a = 4.1484980583161675E - 3$

is the one given in Table 2. In the next section we will come back to this figure.

2.1. Non-linear approximation of the stable manifold

In the previous section, we have discussed how the linear approximation of the stable direction (obtained using the linearisation of the flow) can be used to globalise and parametrise the stable manifold of a periodic halo orbit. In a second approach we have used a non-linear approximation of the stable manifold. In the case of halo orbits and using the parameters mentioned in the preceding section, the results obtained with the linear approximation and the ones using the non-linear one are almost the same. Since the increase in computational cost does not give any extra advantage, all the computations that we present have been done using the linear approximation of the manifolds. However this non-linear study is very useful when dealing with the study of the TCM problem for Lissajous libration point trajectories, specially with big amplitudes.

Following [1], in this section we summarise the procedure for the computation of the non-linear approximation of the stable manifold for the Lissajous and halo orbits. Consider the linearised equations of the restricted three body problem around any collinear equilibrium point

$$\ddot{x} - 2\dot{y} - (1 + 2c_2)x = 0,$$

$$\ddot{y} + 2\dot{x} + (c_2 - 1)y = 0,$$

$$\ddot{z} + c_2z = 0,$$

where c_2 is a parameter depending on the mass ratio and the equilibrium point considered (see [12]). The solution of these equations is given by,

$$x = \alpha_1 e^{\lambda_0 t} + \alpha_2 e^{-\lambda_0 t} + \alpha_3 \cos(\omega_0 t + \phi_1),$$

$$y = \bar{k}_2 \alpha_1 e^{\lambda_0 t} - \bar{k}_2 \alpha_2 e^{-\lambda_0 t} + \bar{k}_1 \alpha_3 \sin(\omega_0 t + \phi_1),$$

$$z = \alpha_4 \cos(v_0 t + \phi_2),$$

where $\bar{k}_1, \bar{k}_2, \omega_0, v_0$ and λ_0 are constants which can be written in terms of c_2 . Finally, α_i and ϕ_i are free amplitudes and phases.

Taking $\alpha_1 = \alpha_2 = 0$ we get libration solutions. In case that $\alpha_1 \neq 0$ or $\alpha_2 \neq 0$ we get exponentially increasing or decreasing translations along privileged directions in the phase space. So, we can consider them as amplitudes in the unstable and stable directions, respectively. In particular, setting $\alpha_1 = 0$, we get initial conditions for orbits in the stable manifold of a certain linear Lissajous orbit corresponding to the linear equations.

Using a Lindsted–Poincaré procedure we can look for a formal series solution of the non-linear equations in terms of the four amplitudes α_i and the following three variables:

$$\theta_1 = \omega t + \phi_1, \quad \theta_2 = \nu t + \phi_2, \quad \theta_3 = \lambda t.$$

These expansions are given by

$$\begin{aligned} \begin{Bmatrix} x \\ y \\ z \end{Bmatrix} &= \sum e^{(i-j)\theta_3} \left[\begin{Bmatrix} x_c \\ y_c \\ z_c \end{Bmatrix}_{ijkm}^{pq} \cos(p\theta_1 + q\theta_2) \right. \\ &\quad \left. + \begin{Bmatrix} x_s \\ y_s \\ z_s \end{Bmatrix}_{ijkm}^{pq} \sin(p\theta_1 + q\theta_2) \right] \alpha_1^i \alpha_2^j \alpha_3^k \alpha_4^m, \end{aligned}$$

where summation is taken with respect to the integer index i, j, k, m, p and q in a suitable way. Also, according to the Lindstedt–Poincaré procedure, in order to avoid secular terms the frequencies ω, ν and λ must be expanded in formal power series of the four amplitudes,

$$\omega = \sum \omega_{ijkm} \alpha_1^i \alpha_2^j \alpha_3^k \alpha_4^m,$$

$$\nu = \sum \nu_{ijkm} \alpha_1^i \alpha_2^j \alpha_3^k \alpha_4^m,$$

$$\lambda = \sum \lambda_{ijkm} \alpha_1^i \alpha_2^j \alpha_3^k \alpha_4^m,$$

being the independent terms, $\omega_{0000} = \omega_0, \nu_{0000} = \nu_0$ and $\lambda_{0000} = \lambda_0$. So the expansions truncated at first

order reproduce the solution of the linear equations of motion. Moreover, if we skip the terms of the expansion related with i and j (this is $i - j \neq 0$) we have expansions for Lissajous orbits but not for their invariant manifolds which turn out to be the same as the ones given in [5].

In the halo periodic case the procedure must be slightly modified. The solution depends only on one frequency and this fact introduces a relation between the two central amplitudes α_3 and α_4 . The formal series expansion are given by,

$$\begin{pmatrix} x \\ y \\ z \end{pmatrix} = \sum e^{(i-j)\theta_3} \left[\begin{pmatrix} x_c \\ y_c \\ z_c \end{pmatrix}_{ijkm}^{pq} \cos(p\theta_1) + \begin{pmatrix} x_s \\ y_s \\ z_s \end{pmatrix}_{ijkm}^{pq} \sin(p\theta_1) \right] \alpha_1^i \alpha_2^j \alpha_3^k \alpha_4^m,$$

where again,

$$\theta_1 = \omega t + \phi_1, \quad \theta_3 = \lambda t,$$

$$\omega = \sum \omega_{ijkm} \alpha_1^i \alpha_2^j \alpha_3^k \alpha_4^m,$$

$$\lambda = \sum \lambda_{ijkm} \alpha_1^i \alpha_2^j \alpha_3^k \alpha_4^m,$$

but now one must take into account a relation between amplitudes which is given by a series expansion of the type

$$\sum d_{ijkm} \alpha_1^i \alpha_2^j \alpha_3^k \alpha_4^m = 0.$$

In all these expansions there are symmetries which make many of the coefficients zero. This fact saves storage and computing time. In [2] the Lissajous expansions have been tested. Using order 25 (i.e. terms up to $i + j + k + m = 25$), differences less than 100 km between the numerically integrated solution and the direct evaluation of the expansion are obtained for the orbits of the manifolds up to about a distance of 500 000 km from the Lissajous orbit.

3. Simulations modifying the modulus of the velocity

3.1. Fixing the arrival point and the time of flight

For the first study of the cost of the TCM, we have taken $t_1 = 4$ days and $\varepsilon = -3$ m/s. For the time of flight we have used the values obtained in [13] for

the optimal solution, this is $t_3 = 173.25$ days. Since the arrival point is not explicitly given in the above reference, we have used the following approximation (which corresponds to integrate the reference initial state during 173.25 days).

As it has already been said, with the values of these parameters fixed, we get a one dimensional set of possibilities, which are the ones displayed in Fig. 4. In the figure, we show the cost of the two TCM, as well as the total cost, in front of the epoch of execution of the second manoeuvre, t_2 . Several remarks should be done in connection with the figure:

- The solutions of Eq. (2) are grouped along, at least, three curves. For $t_2 = 99.5$ days there is a double point in the cost function, corresponding to two different possibilities. In Fig. 5 we have represented both as well as the orbit of the stable manifold where we perform the injection. The qualitative behaviour of both solutions is rather different.
- For $t_2 = 113$ days we get the optimum solution in terms of fuel consumption: $\|\Delta v_1\| + \|\Delta v_2\| = 49.31$ m/s. This value is very close to the one given in [13] for the MOI approach, which is 49.1817 m/s. The discrepancies can be attributed to slight differences between the two nominal orbits and the corresponding target points.
- When t_2 is small or very close to the final time, t_3 , the total cost of the TCMs increases, as it should be expected.
- Around the values $t_2 = 92, 97$ and 102 days, the total cost increases abruptly. This sudden grow is analogous to the one described in [8] in connection with the TCM problem for the Genesis mission. It is also similar to the behaviour found in [16] for the cost of the transfer to a Lissajous orbit around L_2 , when the time of flight between the departure and the injection in the stable manifold is fixed. To explain this fact, we have computed the angle between the two velocity vectors at $t = t_2$, this is when changing from the second to the third leg of the transfer path. This angle has been represented in Fig. 6 from which we see that it also increases sharply at the corresponding epochs. This seems to be the geometrical reason for the detected behaviour.

As a second step, we have done a first parametric study allowing variations in the epoch of the execu-

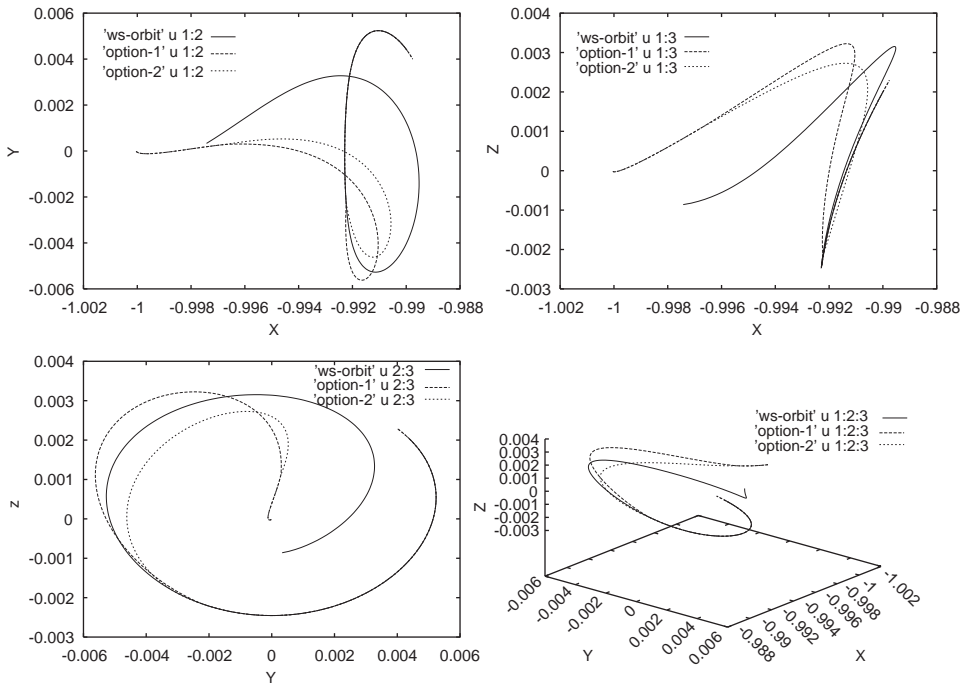


Fig. 5. Coordinate projections and 3D representation of the two solutions obtained for $t_2 = 99.5$ days (double point of the cost function). In the figures we have represented also the orbit of the stable manifold of the nominal orbit where we perform the injection.

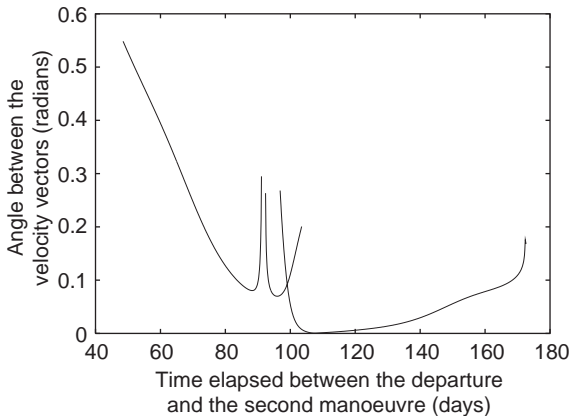


Fig. 6. Using the values of the parameters to get Fig. 4, here we represent the angle (in radians) between the two velocity vectors, the ones just prior and after the TCM2 epoch.

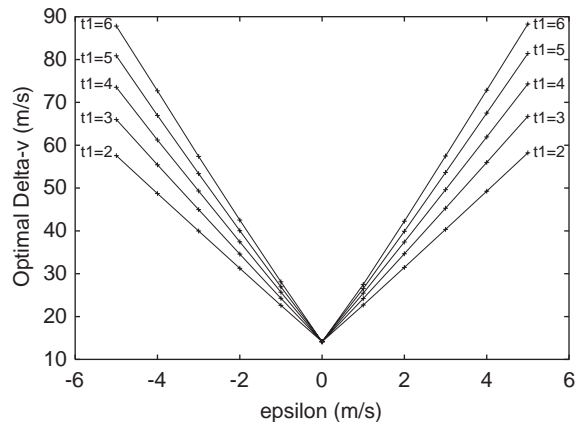


Fig. 7. Behaviour of the optimal cost vs. ϵ for different values of t_1 .

tion of TCM1, t_1 , and in ϵ . Partial results are given in Table 3. In the last column of this table we include the numerical results obtained by Serban et al. [13] for

the MOI strategy (those corresponding to HOI trajectories are similar), which are very close to ours. From this table, it is clearly seen that the behaviour of the optimal cost with respect to ϵ is linear. In Fig. 7 we

Table 3
Numerical results of the parametric study of the TCM cost

t_1	ε	$\ \Delta v_1\ $	$\ \Delta v_2\ $	$\ \Delta v_1\ + \ \Delta v_2\ $	Δv_{opt} [13]
3	5	51.4551	15.2748	66.7299	
3	4	41.2822	14.7060	55.9882	
3	3	31.0891	14.1944	45.2835	
3	2	20.8642	13.7963	34.6605	
3	1	10.5610	13.6390	24.2000	
3	0	0.0974	14.0324	14.1298	
3	-1	10.8051	13.4634	24.2685	
3	-2	21.7421	12.8390	34.5811	
3	-3	32.7661	12.2004	44.9665	45.1427
3	-4	43.8878	11.5459	55.4337	55.6387
3	-5	55.1127	10.8796	65.9923	65.9416
4	5	59.0547	15.2508	74.3055	
4	4	47.4145	14.5247	61.9392	
4	3	35.7505	13.8649	49.6154	
4	2	24.0530	13.3523	37.4053	
4	1	12.2530	13.1986	25.4516	
4	0	0.0987	14.0261	14.1248	
4	-1	12.7285	12.9531	25.6816	
4	-2	25.5010	11.9398	37.4408	
4	-3	38.3502	10.9663	49.3165	49.1817
4	-4	51.3480	9.8576	61.2056	61.5221
4	-5	64.5745	8.9561	73.5306	73.4862
5	5	66.1938	15.2117	81.4055	
5	4	53.1763	14.3203	67.4966	
5	3	40.1315	13.4972	53.6287	
5	2	27.0602	12.8413	39.9015	
5	1	13.8820	12.6547	26.5367	
5	0	0.1172	14.0080	14.1252	
5	-1	14.6289	12.3175	26.9464	
5	-2	29.1862	10.8579	40.0441	
5	-3	43.8275	9.5245	53.3520	53.9072
5	-4	58.8400	8.1134	66.9534	66.8668
5	-5	74.2527	6.6145	80.8672	81.1679

The simulations have been done fixing the arrival point as in Table 2 and the total time of flight $t_3 = 173.25$ days in order to compare the results with the ones obtained in [13] which are displayed in the last column.

represent the results corresponding to a larger set of explorations, where we allow variations in the magnitude of the error, ε , and in the epoch t_1 . From it, it is also clear a linear behaviour of the optimal cost with respect to t_1 .

In the next step of our study we allow variations in the parameter along the orbit. Assuming the periodic halo orbit parametrised by time (the period of the orbit is approximately equal to 180 days) we have taken

a total number of “arrival points” equal to 36, evenly spaced in time. In Fig. 8 we show the behaviour of the total cost of the trajectory correction manoeuvres when the parameter along the orbit is changed around the value corresponding to the optimal solution (which is also displayed in the figure). In the left plot the displayed curves correspond to adding 5, 10 and 15 days, respectively, to the parameter along the orbit and the one in the right-hand side to decrease this parameter

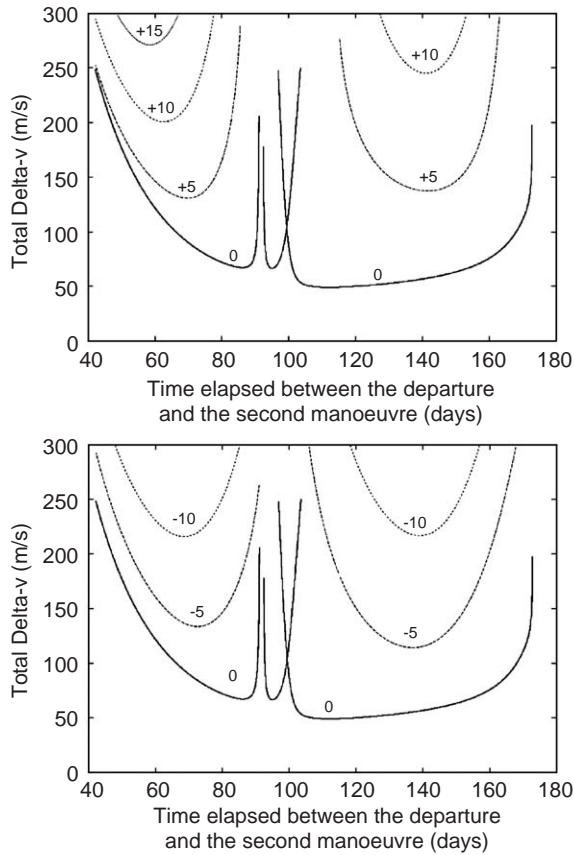


Fig. 8. Total cost of the trajectory correction manoeuvres when the “arrival” point at the halo orbit is changed. Numerical results correspond to changing the arrival point by adding (top figure) or subtracting (bottom figure) 5, 10 and 15 days to the parameter along the orbit corresponding to the optimal solution which is represented by the lowest curve.

in 5 and 10 days. We represent only TCM with a total $\|\Delta v\| = \|\Delta v_1\| + \|\Delta v_2\|$ smaller than 300 m/s. Increasing or decreasing the values of the parameter along the orbit out of the range of the ones represented in the figures, the total cost increases, and the results obtained are always over the threshold fixed for the representation. This is also the reason why one of the three pieces of the optimal solution has disappeared from the plots. In Fig. 9 we plot the surface representing the cost when changing the parameter along the orbit (the value 0 of this parameter corresponds to the point X_a given in Table 2). Since the total time of flight has

been fixed, we get only total TCM costs below 300 m/s within the ranges displayed in the figures.

3.2. Free time of flight

To start with, we take $t_1 = 4$ days, $\varepsilon = -3$ m/s and the arrival point of the preceding sections. With all these parameters fixed, the transfer condition (2) has a two-dimensional set of solutions, which can be parametrised by t_2 and the parameter along the flow, $t_{ws} = t_3 - t_2$, which give the insertion point into the stable manifold. In Fig. 10 we show some sections of this surface, for different values of the parameter along the flow, t_{ws} ranging from 40 days (right curve) to 125 days (left curve) as well as the solution that we have obtained in the preceding section for $t_3 = 173.25$ days. Several remarks should be done with respect to this figure:

- There are values of t_2 and t_{ws} (for instance $t_2 = 108.125$, $t_{ws} = 65$ days) for which the total cost is less than the values we have obtained for $t_3 = 173.25$ days.
- If we take into consideration that the curves we have plotted in Fig. 10 correspond to evenly spaced values of t_{ws} , it seems that the value of t_2 that makes the cost optimal is a linear function of t_{ws} , at least in the right-hand side of the figure where we are close to the optimum values ($t_2 > 100$; the curves in this region correspond to values of t_{ws} equal to 70, 65, 60, 55, 50, 45 and 40 days). Assuming $t_2 = m(t_{ws} - t_{ws}^0) + t_2^0$ the value of m is close to minus one, since the couple (t_2, t_{ws}) that makes minimum the cost verifies $t_{ws} + t_2 \simeq 173.3$ days. This fact justifies why the cost function we obtain for $t_3 = 173.25$ days is very close to the optimal solution when leaving t_3 free.

To study the influence of the variations in the parameter along the orbit, which is equivalent to change the arrival point, we have taken 12 arrival points evenly spaced in time, displayed in Fig. 11. In Fig. 12(a) we show the behaviour of the optimal cost for the first six values of the parameter along the orbit. After point number six, the cost function increases sharply and we have not represented the results associated to them. We see that in the region between the 4th and 5th point there is an optimal solution. Taking values of the

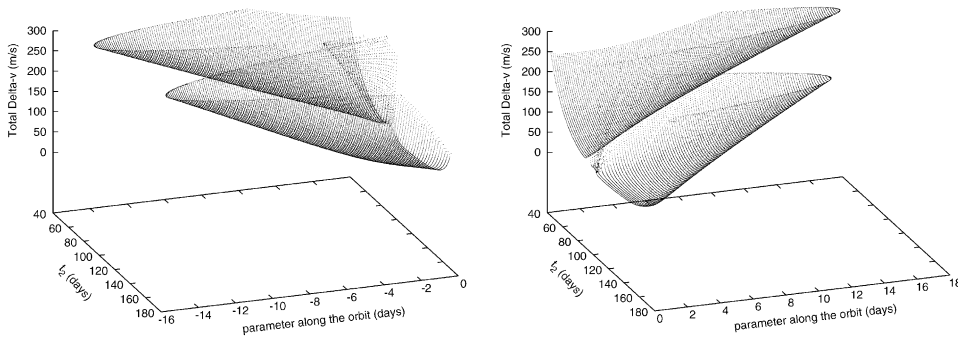


Fig. 9. Total cost of the trajectory correction manoeuvres when the “arrival” point, represented by the parameter along the orbit, is moved around the point X_a given in Table 2, the total time of flight is fixed to 173.25 days and the first manoeuvre is delayed 4 days after the departure. We display the results for negative and positive variations of the parameter along the orbit on the left and right-hand side figures, respectively.

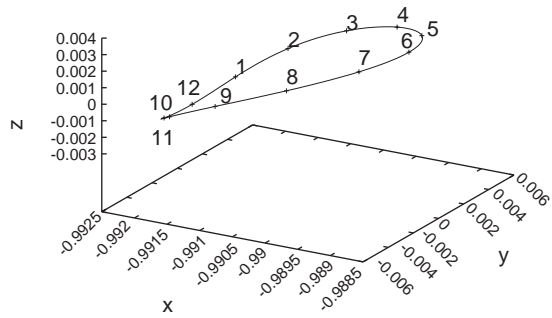
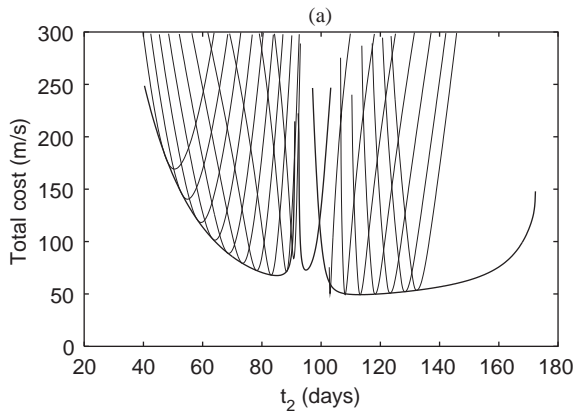


Fig. 11. 3D representation of the nominal halo orbit and the 12 “arrival points”, evenly spaced in time, that have been used in our simulation.

Fig. 10. The curves appearing in the figure are slices of the surface representing the minimum total cost of the TCM, for different values of t_{ws} . In the computations, the first manoeuvre has been delayed 4 days after the departure, the total time of flight is free and the arrival point is fixed. The lowest curve, which almost envelopes the different slices, is the cost function when the total time of flight is fixed to 173.25 days.

parameter along the orbit between these two ones, in Fig. 12(b) we show the curves of minimum cost as a function of t_{ws} . Each curve corresponds to a different value of the parameter along the orbit varying between 0.8 and 1.6 (with step 0.1).

As before, it is interesting to observe that the values of t_2 and t_{ws} that minimise the total cost behave linearly, with respect to the parameter along the orbit, when we are near to the optimal solution. This

is shown in Figs. 12(c) and (d). Using this fact we have obtained that the optimal solution corresponds to $t_h = 61.34$ days with a total cost of 49.186 m/s. The insertion manoeuvre takes place 111.14 days after the departure with a total time of flight of 172.27 days. This optimal solution is displayed in Fig. 13.

As a final exploration we allow variations in the size of the target halo orbit. We have done the computations using halo orbits with values of the z -amplitude β equal to 0.08 and 0.18 in addition to the value 0.28 used in the preceding simulations. In Table 4 we give the results obtained using the same nominal departure point for all of them. We remark that when the amplitude of the nominal orbit decreases, the total cost of the optimal TCM increases as well as the value of the

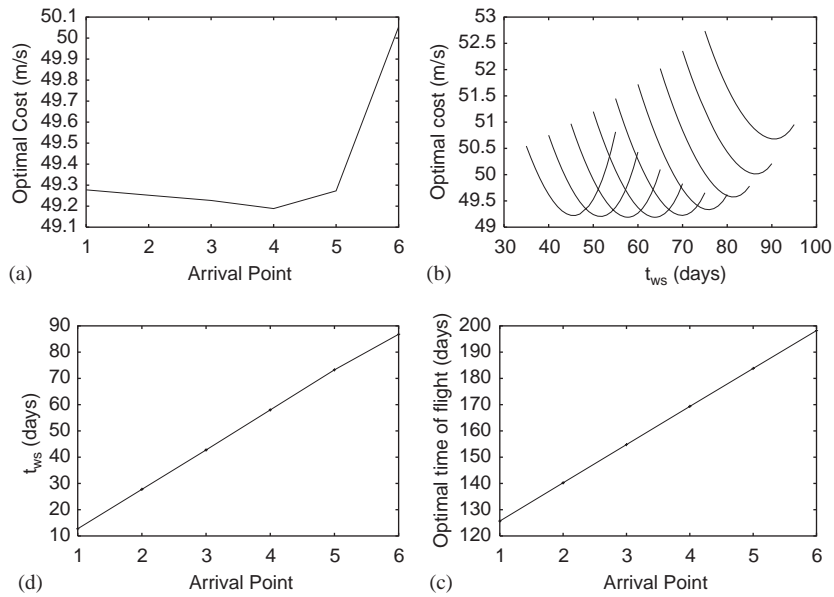


Fig. 12. (a) Minimum total cost of the trajectory correction manoeuvres when the first manoeuvre is delayed 4 days, $\varepsilon = -3$ m/s, the total time of flight is free and the arrival point is varied. (b) Section of the cost surface for different values of the parameter along the orbit between the 4th and 5th arrival point. (c) Optimal time between the insertion into the stable manifold and the arrival when the arrival point is varied. (d) Optimal time of flight when the arrival point is varied.

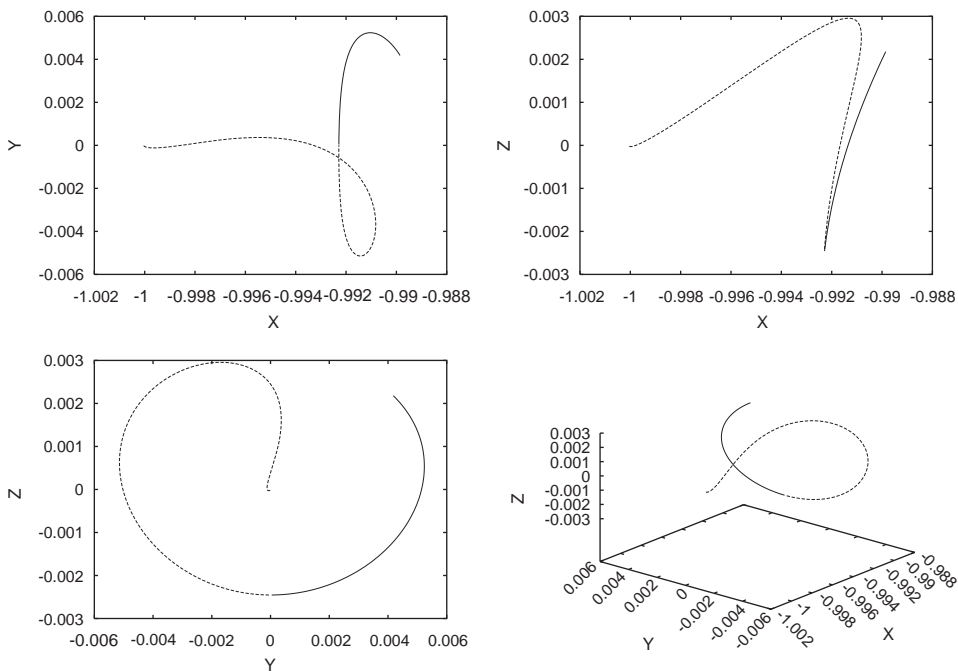


Fig. 13. Projections and 3D representation of the optimal transfer trajectory with $t_2 = 111.14$ days, $t_{ws} = 61.13$ days and total $\delta v = 49.186$ m/s.

parameter along the flow (t_{ws}) which corresponds to the optimal solution.

3.3. Departing from the stable manifold

In this section we show the results corresponding to take the departure point on the stable manifold of the target orbit. Now, instead of using the departure conditions given in Table 1, we take as initial position and velocity a point on the stable manifold, with the velocity components affected by some error. If the

Table 4
Optimal solution for different normalised z -amplitude (β) halo orbits

β	0.28	0.18	0.08
t_2 (days)	111.14	146.61	69.70
t_{ws} (days)	61.13	111.55	156.80
Cost (m/s)	49.186	97.055	170.965

The departure point has been taken as in Table 1

error is set equal to zero, then no TCM is needed to reach the target orbit.

We use the same nominal halo orbit of the preceding sections, this is, a halo orbit around the L_1 point of the Earth–Sun system, with normalised z -amplitude $\beta=0.28$. Taking the parameter along the orbit between $[0, 2\pi]$, in Fig. 14 we represent the minimum distance to the Earth of the stable manifold of the nominal orbit at its first close passage following the parameter along the flow. As it can be seen, there are orbits which collide with the Earth (the minimum distance to the Earth is below the equatorial radius). The departure point has been selected on the orbit associated to the parameter along the orbit equal to $t_h = 3.66000$ when its distance from the centre of the Earth is 6578 km. The adimensional coordinates of this point are given in Table 5 and, as it can be seen, are not too far from those given in Table 1.

Now, adding $\varepsilon = 7$ m/s to the three velocity components of the nominal point given in Table 5, we

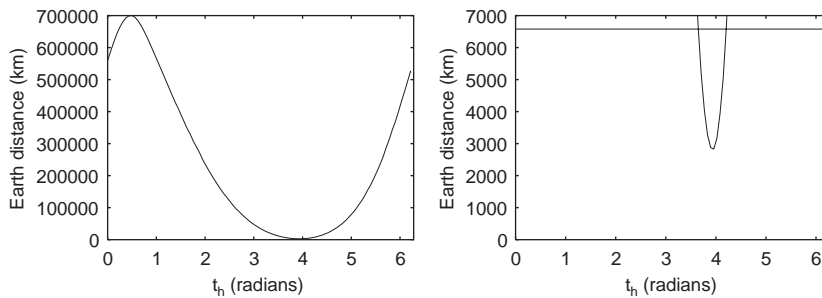


Fig. 14. Minimum distance to the Earth of the orbits of the stable manifold of the nominal halo orbit with $\beta=0.28$. The distance is below 6578 km for the values of the parameter along the orbit (with values in $[0, 2\pi]$) t_h between 3.648511 and 4.207157 as can be seen in the magnification.

Table 5
Adimensional coordinates of the nominal departure point on the stable manifold

$x_0^{nom} = -1.000036453220198E + 0$	$\dot{x}_0^{nom} = 1.618213815598005E - 1$
$y_0^{nom} = -9.466006191933124E - 6$	$\dot{y}_0^{nom} = -2.526026481278061E - 1$
$z_0^{nom} = -1.128673413649424E - 5$	$\dot{z}_0^{nom} = -2.308399055627169E - 1$

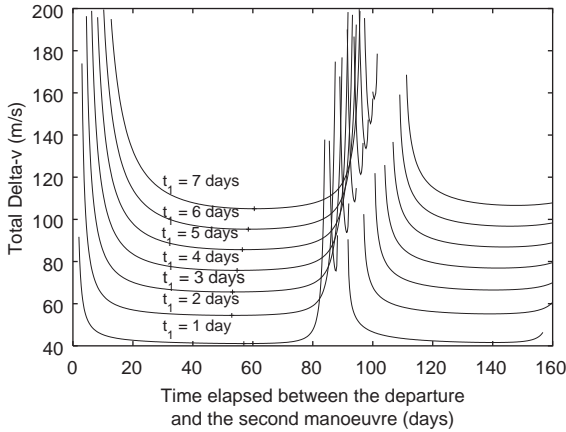


Fig. 15. Total cost of the TCM, as a function of t_2 , for different values of t_1 . On each curve, the points with a cross correspond to the optimal cost.

compute the departure point which will be used for the explorations (the parametric study varying the value of ε gives results qualitatively analogous to the ones already described). As time of flight we take the value $t_3 = 217.28$, which is the total time required by the orbit with the initial conditions given in Table 5 to reach the arrival point, X_a , at the halo orbit (always at a distance of 200 km, in the direction of the stable manifold). In Fig. 15 we show the total cost (in m/s) of the TCM as a function of t_2 , for different values of t_1 between 1 and 7 days. On each curve we have marked with a cross the points corresponding to the minimum cost. From this figure one clearly sees that:

1. As t_1 increases, the cost of TCMs also does, and it behaves almost linearly with respect to t_1 in the selected range.
2. The cost of the TCMs is about a 20% less than the values given in Table 3, when the departure point is not taken on the stable manifold.
3. The optimal values of t_2 move around $t_2 = 58$ days, and approximately after 82 days ($t_2 = 140$ days) one finds also values for TCM1 very close to the optimal ones.

As a final exploration we allow variations of the insertion point along the stable manifold. In particular if we fix $t_1 = 1$ day and $t_2 = 57$ days, we get a target insertion point on the stable manifold, which corre-

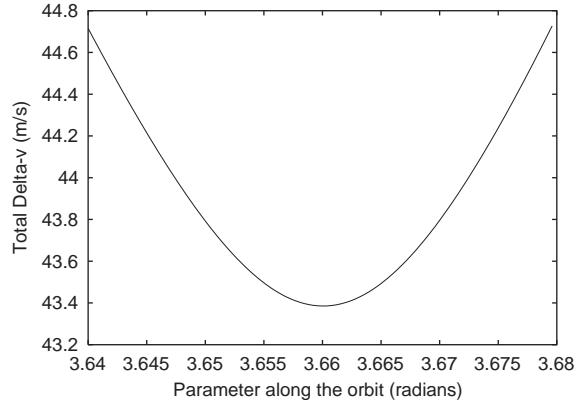


Fig. 16. Total cost of the TCM for different values of the parameter along the orbit.

sponds to a parameter along the orbit approximately equal to 3.66. Now, we have allowed values of the parameter along the orbit between 3.64 and 3.68 and we have studied the total cost of the TCM, keeping fixed the values of t_1 and t_2 , and taking as insertion point the one at minimum distance to the target point of insertion already described. The results are given in Fig. 16, from which we see that the cost increases when we move away from the most “natural” trajectory.

4. Simulations modifying the direction of the insertion manoeuvre

In this section we study the influence stressed on the cost function by the presence of errors not only in the modulus, but also in the direction of the nominal transfer orbit insertion manoeuvre. For such purpose we have proceeded as follows. Having fixed the departure and arrival states, the total time of flight and the delay of the first manoeuvre, we modify the velocity of the initial condition according to

$$\vec{v}(0) = \vec{v}_0^{\text{ref}} + \Delta\vec{v}_0,$$

where, as was mentioned in Section 2, $\Delta\vec{v}_0$ is a point over an ellipsoid with semi-axes $a = \alpha\sigma$, $b = \beta k\sigma$; α and β being random numbers with $N(0, 1)$ distribution and σ , k two parameters that take into account the down-track and cross-track errors of the manoeuvre, respectively. We have set $\sigma = 7$ m/s and $k = \frac{1}{3}$

Table 6

Statistics of the minimum Δv (m/s) values obtained in the Monte-Carlo simulations when we take the departure and arrival states as in Tables 1 and 2, respectively, and fix the total time of flight to 172.25 days

Branch 1				Branch 3			
Delay (days)	Range	Average	Standard deviation	Delay (days)	Range	Average	Standard deviation
1.0	45.8272–54.6310	48.2453	2.2399	1.0	32.2817–43.8993	34.7027	2.8358
1.5	43.8032–67.2710	48.0029	6.2628	1.5	32.1943–60.1267	37.7074	7.6498
2.0	42.2079–67.5460	46.2787	5.4225	2.0	32.4934–63.1765	37.9129	6.7319
2.5	40.9965–61.4381	44.3796	4.0005	2.5	32.9850–58.9597	38.1174	5.5727
3.0	39.8787–67.7844	44.2993	5.6430	3.0	34.0776–67.9567	40.0730	7.2321
3.5	39.2465–66.2347	44.1344	6.9594	3.5	35.4637–67.4763	41.9438	8.4529
4.0	38.6205–54.6568	43.1542	4.6470	4.0	37.7362–56.0575	43.1814	5.2771
4.5	37.9201–65.6453	42.7291	6.2320	4.5	38.1161–67.9855	43.5183	6.6162
5.0	37.1995–58.8220	41.6158	4.9046	5.0	31.0833–61.3658	42.2114	5.9583

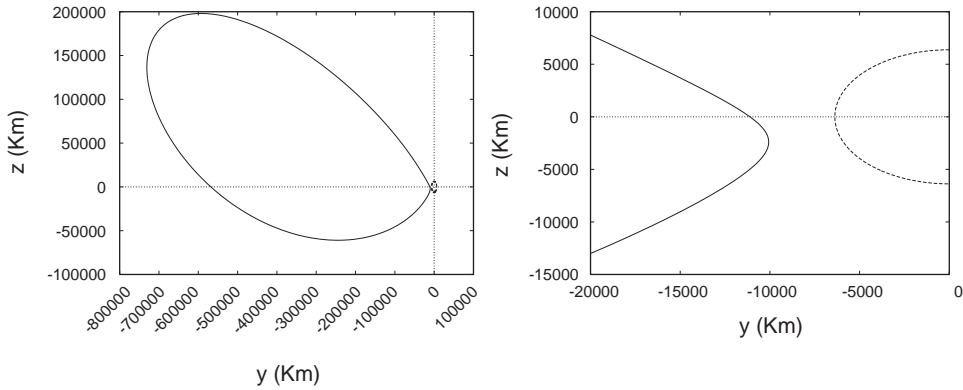


Fig. 17. Intersection of the stable manifold of the halo orbit of z -amplitude $\beta = 0.2$ with the plane $x = -1 + \mu$. The right-hand side figure shows an enlargement of the manifold near the Earth.

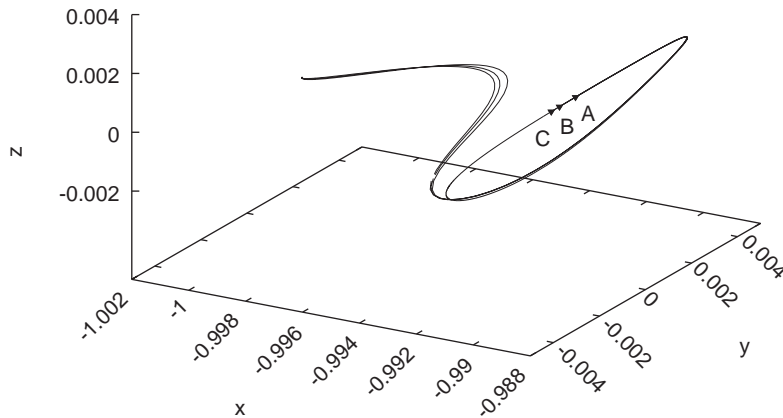


Fig. 18. Transfer trajectories on the stable manifold of the halo orbit with z -amplitude $\beta = 0.2$ used for the Monte-Carlo simulations. The value of the parameter along the orbit corresponding to the points A, B and C are $0.575T$, $0.590T$ and $0.600T$, respectively, where T is the period of the halo orbit and the origin has been taken at $y = 0, \dot{z} > 0$.

Table 7

Departure states (in adimensional coordinates) used for the Monte-Carlo simulations

A	$x_0^{\text{nom}} = -1.0000386161014463E + 0$ $y_0^{\text{nom}} = -1.09712123358261351E - 5$ $z_0^{\text{nom}} = -1.2104617096724314E - 5$	$\dot{x}_0^{\text{nom}} = 1.0568853431987743E - 1$ $\dot{y}_0^{\text{nom}} = -3.4859939402723461E - 1$ $\dot{z}_0^{\text{nom}} = -4.6976851370853528E - 2$
B	$x_0^{\text{nom}} = -1.0000373525314581E + 0$ $y_0^{\text{nom}} = -1.1332225221510923E - 5$ $z_0^{\text{nom}} = -1.1805124837192875E - 5$	$\dot{x}_0^{\text{nom}} = 9.3096407087278496E - 2$ $\dot{y}_0^{\text{nom}} = -3.6028772745978449E - 1$ $\dot{z}_0^{\text{nom}} = -6.9359674065761412E - 3$
C	$x_0^{\text{nom}} = -1.0000383052579993E + 0$ $y_0^{\text{nom}} = -9.6884694784905050E - 6$ $z_0^{\text{nom}} = -1.1796329800593463E - 5$	$\dot{x}_0^{\text{nom}} = 7.3933907053329612E - 2$ $\dot{y}_0^{\text{nom}} = -3.6223834931003152E - 1$ $\dot{z}_0^{\text{nom}} = 1.6867375755366110E - 2$

These states correspond to the orbits of the stable manifold of the halo orbit with z -amplitude $\beta = 0.2$ displayed in Fig. 18.

Table 8

Statistics of the minimum Δv (m/s) values obtained in the Monte-Carlo simulations for the three transfer trajectories given in Table 7

Dept. point	Branch 1				Branch 3			
	Delay (days)	Range	Average	Standard deviation	Delay (days)	Range	Average	Standard deviation
A	1.0	0.3067–31.2725	5.1594	6.0159	1.0	0.3158–31.5863	5.2130	6.0748
A	1.5	0.0220–29.9299	8.0556	7.3834	1.5	0.0237–30.2711	8.1493	7.4693
A	2.0	0.1977–38.9858	8.5953	8.8344	2.0	0.2290–39.4471	8.6955	8.9393
A	2.5	0.2368–35.0906	7.1188	7.4092	2.5	0.2421–35.5233	7.2123	7.5069
A	3.0	0.2462–51.4257	6.9843	9.9216	3.0	0.2519–52.2075	7.0869	10.0723
A	3.5	0.0078–49.1599	12.5384	13.2554	3.5	0.0078–49.9641	12.7300	13.4629
A	4.0	0.4595–40.9719	9.9559	10.1909	4.0	0.4847–41.6886	10.1189	10.3584
A	4.5	0.1579–43.6470	9.6663	8.5092	4.5	0.1698–44.3944	9.8256	8.6595
A	5.0	0.0558–59.2407	13.7203	15.3319	5.0	0.0654–60.3038	13.9663	15.6089
B	1.0	0.1787–24.5104	4.7244	4.7987	1.0	0.1797–24.7175	4.7687	4.8412
B	1.5	0.0237–31.7087	7.1222	7.3545	1.5	0.0295–32.0806	7.2039	7.4395
B	2.0	0.0978–28.2246	8.3327	7.8268	2.0	0.0990–28.5629	8.4356	7.9212
B	2.5	0.2774–53.0985	11.0393	10.8917	2.5	0.2875–53.8095	11.1871	11.0352
B	3.0	0.0416–34.4593	10.6114	8.8839	3.0	0.0420–34.9877	10.7649	9.0192
B	3.5	0.1073–48.5955	12.2914	11.9300	3.5	0.1299–49.3598	12.4807	12.1153
B	4.0	0.5204–81.5386	14.8066	16.4807	4.0	0.5359–82.8874	15.0497	16.7499
B	4.5	0.1269–36.1104	9.9189	10.1927	4.5	0.1326–36.6636	10.0789	10.3617
B	5.0	0.3128–74.6056	11.7691	13.6624	5.0	0.3211–75.9197	11.9756	13.9051
C	1.0	0.0166–45.1383	6.4758	8.7325	1.0	0.0188–45.5852	6.5369	8.8143
C	1.5	0.0176–31.6232	5.1243	6.4732	1.5	0.0214–31.9820	5.1844	6.5447
C	2.0	0.1314–27.1217	7.0244	7.4897	2.0	0.1314–27.4705	7.1141	7.5821
C	2.5	0.3346–40.1814	8.5940	10.0078	2.5	0.3748–40.7319	8.7083	10.1432
C	3.0	0.0917–29.2028	6.5931	7.0039	3.0	0.0965–29.6340	6.6849	7.1048
C	3.5	0.0899–45.6374	10.0596	9.7600	3.5	0.0963–46.3355	10.2139	9.9141
C	4.0	0.4678–50.5522	11.3490	10.7619	4.0	0.4755–51.3729	11.5314	10.9408
C	4.5	0.0753–57.4763	11.1074	12.3864	4.5	0.0773–58.5060	11.2949	12.6023
C	5.0	0.3643–43.8067	11.6430	12.1151	5.0	0.3676–44.5589	11.8491	12.3278

The total time of flight t_3 is approximately equal to 205.506, 206.925 and 207.566 if the transfer trajectory is A, B, C, respectively.

through all the simulations. Using these data, we have performed Monte-Carlo simulations using 100 different choices of $\Delta\vec{v}_0$.

As a first example, let us consider fixed the initial and final states, with the values given in Tables 1 and 2, respectively, as well as the total time of flight to 173.25 days. As was shown in Fig. 4, the cost function displays three branches, each with a local minimum. With these values, we have done several Monte-Carlo explorations with different values of the time delay in the execution of the first correction manoeuvre. The results are given in Table 6. In this table we give the rank of variation of the minimum cost, together with the average value and the standard deviation, for the first and third branches. We have not taken into consideration the central branch since the actual values attained within this region are always larger than those of the other two branches and, often, out of the range of the capabilities of the thrusters.

For the remaining explorations we have considered three different transfer orbits, all of them on the stable manifold of the halo orbit of normalised z -amplitude $\beta=0.2$. The stable manifold of this orbit comes close to the Earth but without colliding with it. Fig. 17 shows the cross-section of the stable manifold, with the plane $x = -1 + \mu$.

Taking the parameter along the orbit from $[0, T]$ (T being the period of the orbit), and setting the point of intersection of the orbit with the plane $y=0$ and $\dot{y} > 0$ as the origin, the orbits on the stable manifold corresponding to parameter values in $[23T/40, 121T/200]$ achieve a minimal distance to the Earth between 100 and 320 km. In Fig. 18 we have represented the three orbits selected, which have been labelled as A , B and C and correspond to values of the parameter along the orbit equal to $0.575T$, $0.590T$ and $0.600T$, respectively. The departure states used, corresponding to these three different orbits, are given in Table 7

Table 8 exhibits the results of 50 Monte-Carlo simulations for different time delays for the execution of the first TCM and obtained by fixing the arrival state to the previously mentioned A , B and C points. The departure chosen thereof was the point, on the corresponding orbit, at a minimum distance to the Earth, and the total time of flight was taken to be the value of the parameter along the flow between both states.

5. Conclusions

1. The TCM problem can be studied just by using simple dynamical systems concepts.
2. For the optimal TCM, the results obtained with this approach agree, qualitatively and quantitatively, with those obtained with the help of optimal control software.
3. For periodic halo orbits, the use of the linear approximation of the stable manifold gives the same results as using the non-linear one.
4. The procedure developed can be used to compute optimal TCM for any kind of libration point orbits.

Acknowledgements

The research of G.G. and J.M. has been partially supported by Grants DGICYT BFM2003–9504 (Spain) and CIRIT 2001 SGR–70 and 2003 XT–00021 (Catalonia). M.M. wishes to acknowledge the support of the doctoral research Grant AP2001–3064 from the Spanish Ministerio de Educación, Cultura y Deportes.

References

- [1] E. Canalias, J. Cobos, J.J. Masdemont, Transfers between Lissajous libration point orbits, *The Journal of the Astronautical Sciences* 51 (2003) 1–50.
- [2] J. Cobos, M. Hechler, FIRST/PLANCK mission analysis: transfer to a Lissajous orbit using the stable manifold, Technical Report MAS, Working Paper No. 412, ESOC, 1998.
- [3] R.W. Farquhar, The control and use of libration point satellites. Technical Report TR R346, Stanford University Report SUDAAR–350, 1968.
- [4] G. Gómez, À. Jorba, J. Masdemont, C. Simó, Study of the transfer from the Earth to a halo orbit around the equilibrium point L_1 , *Celestial Mech.* 56 (1993) 541–562.
- [5] G. Gómez, À. Jorba, J.J. Masdemont, C. Simó, Dynamics and Mission Design Near Libration Point Orbits, vol. 3, *Advanced Methods for Collinear Points*, World Scientific, Singapore, 2001.
- [6] G. Gómez, J. Llibre, R. Martínez, C. Simó, Dynamics and Mission Design Near Libration Point Orbits, vol. 1, *Fundamentals: The Case of Collinear Libration Points*, World Scientific, Singapore, 2001.
- [7] M. Hechler, SOHO mission analysis L_1 transfer trajectory, Technical Report MAO, Working Paper No. 202, ESA, 1984.
- [8] K.C. Howell, B.T. Barden, Brief summary of alternative targeting strategies for TCM1, TCM2 and TCM3, Purdue University, 1999, private communication.

- [9] J.A. Kechichian, The efficient computation of transfer trajectories between earth orbit and L_1 halo orbit within the framework of the Sun–Earth restricted three body problem, AAS/AIAA Space Flight Mechanics Meeting, Clearwater, Florida, USA, AAS Paper 00–174, 2000.
- [10] M.W. Lo, B.G. Williams, W.E. Bollman, D. Han, Y. Hahn, J.L. Bell, E.A. Hirst, R.A. Corwin, P.E. Hong, K.C. Howell, B.T. Barden, R.S. Wilson, Genesis mission design, AIAA Space Flight Mechanics, Paper No. AIAA 98–4468, 1998.
- [11] D.L. Mains, Transfer trajectories from Earth parking orbits to L_1 halo orbits, Master’s Thesis, Department of Aeronautics and Astronautics, Purdue University, Purdue, USA, 1993.
- [12] D.L. Richardson, Analytical construction of periodic orbits about the collinear points, *Celestial Mech.* 22 (1980) 241–253.
- [13] R. Serban, W.S. Koon, M.W. Lo, J.E. Marsden, L.R. Petzold, S.D. Ross, R.S. Wilson, Halo orbit mission correction maneuvers using optimal control, *Automatica* 38 (2002) 571–583.
- [14] R. Serban, L.R. Petzold, COOPT—a software package for optimal control of large-scale differential-algebraic equation systems, *J. Math. Comput. Simulation* 56 (2001) 187–203.
- [15] J. Stoer, R. Boulirsch, *Introduction to Numerical Analysis*, Springer, Berlin, 1983.
- [16] R.S. Wilson, K.C. Howell, M.W. Lo, Optimization of insertion cost transfer trajectories to libration point orbits, *Adv. Astronaut. Sci.* 103 (2000) 1569–1586.